Original Research Article:

High-gamma and beta bursts in the Left Supramarginal Gyrus can accurately differentiate verbal memory states and performance.

Nicolás Sawczuk[1], Daniel Y. Rubinstein[2], Michael R. Sperling[2], Katrina Wendel-Mitoraj[3], Diego F. Slezak[1*], Juan Kamienkowski*[1], Shennan A. Weiss[4*],
[1]Department of Computer Science, University of Buenos Aires, Buenos Aires, Argentina
[2]Department of Neurology and Neuroscience, Thomas Jefferson University, Philadelphia, PA 19107, USA
[3]Soenia by Braincare Oy, Tampere, Finland
[4]Dept. of Neurology, State University of New York Stony Brook, Stony Brook, New York, 11790 USA

*: These authors share senior authorship

Corresponding author: Shennan A. Weiss (shennanweiss@gmail.com)
Address:
101 Nicolls Road Stony Brook, NY 1179
Health Sciences Tower
HSC T12, Room 041
Stony Brook, NY 11794-8121

Abstract

Positive and negative subsequent memory effects have been reported in the left supramarginal gyrus (LSMG) which is thought to mediate attention to memory. We performed a secondary analysis of 142 verbal free recall experiments, in patients with medically refractory epilepsy, undergoing pre-surgical evaluation with electrode contacts implanted in the LSMG. Convolutional neural networks (CNNs), utilizing high-gamma and beta bursts in the LSMG during the word encoding epoch, had an area under the receiver operating curve (AUROC) for classifying remembered words of >0.6 in 16 experiments. These experiments were distinguished by higher peak amplitudes of high-gamma and beta bursts and electrode placement in more anterior and dorsal regions of the LSMG. Among these 16 experiments the CNN utilizing high-gamma and beta bursts was equivalent, or outperformed, the equivalent CNN utilizing raw intracranial electroencephalogram (iEEG). In 7 of these 16 experiments, we also trained and tested CNNs that differentiated verbal word encoding from recall, and better performance recall from poor performance recall. These CNNs also utilized the high-gamma and beta bursts from the respective iEEG epochs. For many of the experiments these CNNs had an AUROC >0.6 demonstrating proof of principle that memorpy state and performance biomarkers can be derived from high-gamma and beta bursts in the iEEG recordings of the LSMG alone.

Highlights:

1) Cross-validated convolutional neural networks (CNNs) utilizing intracranial EEG (iEEG) recorded from the left supramarginal gyrus can label words remembered or forgotten in verbal memory encoding.
2) The cross-validated CNN performs best when trained and tested using iEEG with higher amplitude high-gamma (80-150 Hz) and beta (16-40 Hz) signals.
3) Cross-validated CNNs utilizing only high-gamma and beta bursts can also label encoding and recall epochs and label good recall epochs from poor recall epochs.

Keywords: 1) Verbal memory, 2) Supramarginal gyrus, 3) high-gamma oscillations, 4) beta oscillations, 5) convolutional neural network

Abbreviations

MCI: mild cognitive impairment; iEEG: intracranial electroencephalography; LSMG: left supramarginal gyrus; fMRI: functional magnetic resonance imaging; SME: subsequent memory effect; BOLD: blood oxygen level dependent; FR: verbal free recall task; catFR: categorical verbal free recall task; HG: high-gamma oscillations (80-150 Hz); FIR: finite impulse response filter; CNN: convolutional neural network i.e., “deep learning”; AUROC: Area under the receiver operating curve; AUC: Area under the curve synonymous with AUROC; PPV: positive predictive value; NPV: negative predictive value.

Graphical Abstract:

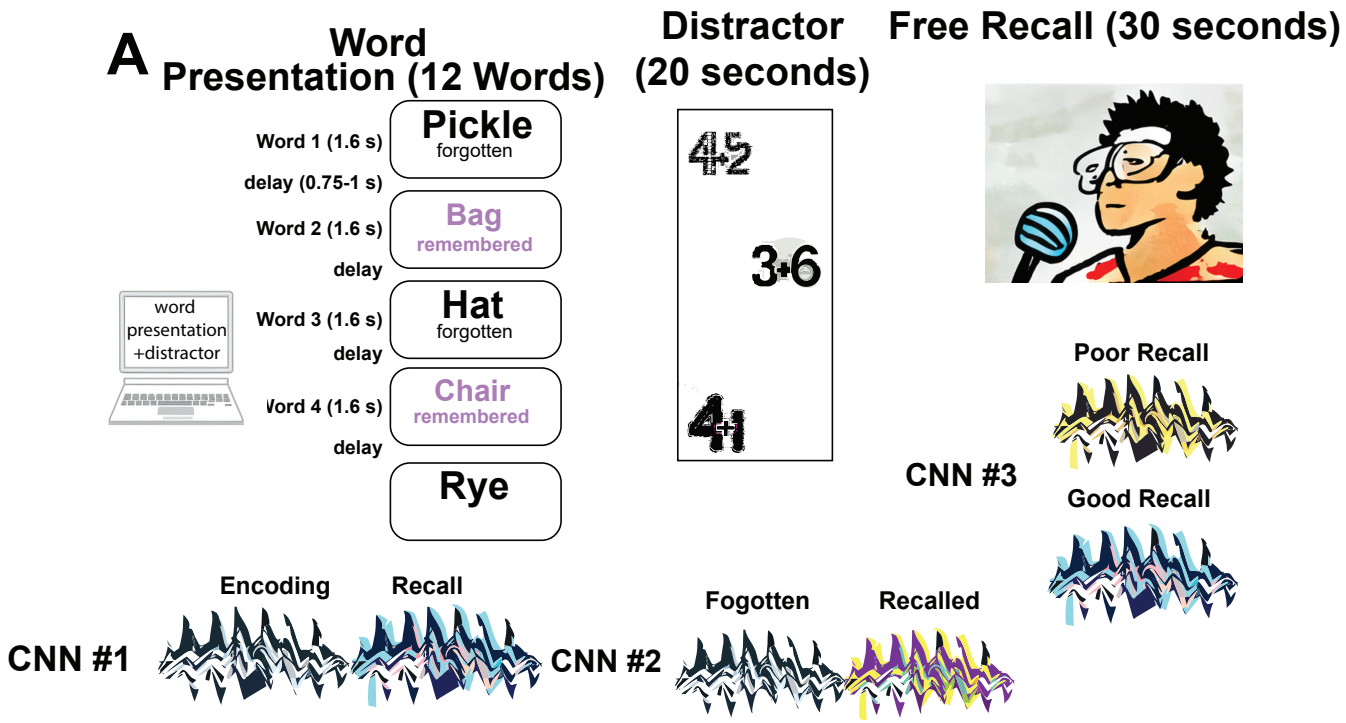

Introduction

The role of invasive technologies in treating 15-20% of the population over 65 years old with mild cognitive impairment (MCI) is not yet established. Herein, we show proof of concept of neurophysiological biomarkers of memory states and performance derived exclusively from intracranial EEG (iEEG) recordings from the Left Supramarginal Gyrus (LSMG-Brodmann area 40). The LSMG is hypothesized to be important in directing attentional resources towards relevant external and internal (*i.e.,* mental) stimuli for promoting memory encoding and retrieval(Cabeza et al., 2008; Ciaramelli et al., 2010, 2008; Sestieri et al., 2017; Uncapher and Wagner, 2009), and is part of the dorsal language network(Yagmurlu et al., 2016) which is analogous to the right hemispheric ventral attention network(Bernard et al., 2020).

Past work utilizing averaged fMRI(Uncapher and Wagner, 2009) and iEEG signals(Rubinstein et al., 2021) show that, for subsequently recalled verbal and visual information, the LSMG signals show subsequent memory effects (SMEs). A SME is when the average recalled memory items' physiological response, as compared to the average forgotten items' response, is significantly larger (*i.e.,* positive) or smaller (*i.e.,* negative). During encoding, BOLD signal in the LSMG exhibits SMEs that can be either positive or negative(Uncapher and Wagner, 2009), and high-gamma power in the LSMG also exhibits a positive SME(Rubinstein et al., 2021). During stimulus recall epochs, BOLD signals(Cabeza et al., 2008; Ciaramelli et al., 2008) and high-gamma power(Gonzalez et al., 2015) also exhibit a positive SME in the LSMG.

We examined 144 subjects diagnosed with medically refractory focal epilepsy undergoing pre-surgical evaluation with depth and subdural electrodes placed, in part, in the LSMG. Electrode contact placement was selected to best delineate the seizure onset zone. During the hospitalization, the subjects participated in a delayed verbal free recall task (Figure 1A, Ezzyat et al., 2018). Convolutional neural networks (CNNs) were trained and tested using either: a) time-series of high-gamma and beta bursts recorded from the LSMG iEEG; or b) the broad-band iEEG from the LSMG, during the task. The three CNN types could either: 1) discriminate encoding from recall epochs during the task (Figure 1B1); 2) discriminate good encoding from poor encoding (*i.e.,* predict that a presented word will be remembered, Figure 1B2); or 3) discriminate good recall from poor recall (*i.e.,* predict that after the delay a relatively larger number of words from the list will be spoken aloud) (Figure 1B3).

Gamma and beta bursts, generated by ensembles of inhibitory interneurons, are implicated in mediating working memory, in the frontal lobe, and the bursts coordinate the activity of excitatory pyramidal cells(Lundqvist et al., 2016; Lundqvist and Wutz, 2022; Miller et al., 2018), while high-gamma bursts are mostly attributable to pyramidal neuron firing and correlate with the BOLD signal(Canolty et al., 2006; Mukamel et al., 2005; Sinai et al., 2005). Thus, we hypothesized that the CNNs trained and tested using high-gamma and beta bursts, solely from the LSMG, during the free recall task would be equally accurate as compared to the CNNs trained using broad-band iEEG in classifying verbal memory state and performance.

Methods

Participants

Patient data were collected as part of a multi-center project named Restoring Active Memory (RAM) https://memory.psych.upenn.edu/Main_Page#Cognitive_Neuromodulation at the following centers: Thomas Jefferson University Hospital (Philadelphia, PA), University of Texas Southwestern Medical Center (Dallas, TX), Emory University Hospital (Atlanta, GA), Dartmouth-Hitchcock Medical Center (Lebanon, NH), Hospital of the University of Pennsylvania (Philadelphia, PA), and Mayo Clinic (Rochester, MN). The research protocol was approved by the Institutional Review Board at each hospital and informed consent was obtained from each participant. A subset of this data previously analyzed in (Rubinstein et al., 2021) and R01 proposal R01MH120161 was utilized by Dr. Weiss and colleagues at SUNY Downstate in accordance with an agreement with Thomas Jefferson University. This data is also available at FR1: https://openneuro.org/datasets/ds004789/versions/3.1.0 catFR1: https://openneuro.org/datasets/ds004809/versions/2.2.0.

For details on the depth and subdural electrodes used, the detailed electrophysiological data acquisition, and the neuroanatomical localization of the electrode contacts see (Ezzyat et al., 2018, 2017). Data was recorded with a minimum sampling rate of 500 Hz. Additionally, iEEG recordings from the LSMG were visually inspected for quality and contaminated and noisy contact recordings were excluded prior to analysis with the convolutional neural networks. Recordings in the dataset that utilized electrical stimulation of the brain were excluded as well.

Verbal memory task

Each subject participated in a delayed free-recall (FR) task. An experimental session consisted of encoding, distractor, and recall epochs. The encoding epoch consisted of twelve words, with each word shown on the screen for 1,600 ms, followed by a blank inter-stimulus interval with a duration between 750–1,000 ms. Immediately following the final 12th word in each list, a distractor task consisting of arithmetic problems was performed for 20 s. Subsequently in the recall epoch, participants were then given 30 s to verbally recall as many words as possible from the list in any order (Figure 1A). Further details can be found in (Ezzyat et al., 2018, 2017). List words in some experiments were categorical (catFR). Subjects completed between 9-24 sessions.

High-gamma (HG) and beta burst amplitude analysis

All experimental sessions were visually analyzed in Micromed™ Brain Quick™. For measuring peak HG amplitude finite impulse response (FIR) band-pass filters between 80-200 Hz were used, and the peak amplitude evaluated using the standard cursor across the recording duration. To measure peak beta amplitude the FIR band-pass filters between 16-30 Hz were used instead followed by evaluation using the standard cursor across the recording duration.

High-gamma (HG) and beta burst analysis

All custom code was written in Python™. The signal from each contact was standardized using StandardScaler (scikit-learn). The topographical analysis of the wavelet convolution(Waldman et al., 2018) was adapted to detect the discrete HG and beta oscillatory bursts in the computed wavelet convolutions of the recording from each contact (Supplementary Figure 1 and 2, Supplementary Methods). The oscillatory bursts were represented with Gaussian kernel functions:

$$f(x) = Ae^{\frac{(x-p)^2}{2*w^2}}$$

where A is the maximum power of each oscillatory burst, p the midpoint between onset and offset time and w the time duration of each oscillatory burst.

Convolutional Neural Network (CNN) Training and Testing

To differentiate between encoding vs recall memory states (Fig 1B1, CNNs #1), the 3-second word encoding trials, and corresponding LSMG iEEG (i.e., trials), were randomly selected from a session of 12 words and combined with 3-second iEEG epochs randomly selected from the session's corresponding 30-second free recall epoch. This randomization reduced the probability that the neurophysiological correlates of speech activity contribute to CNNs #1's training. To differentiate; 1) good and poor encoding (Fig 1B2, CNNs #2); and 2) good and poor recall states (Fig 1B3, CNNs #3), the 30 seconds encoding and recall sessions, respectively, were concatenated at random.

For CNN#2, the signals from each contact were represented by three time-series: 1) the raw iEEG; 2) the beta bursts; and 3) the HG bursts. For CNN#1,3 the signals consisted solely of 1) the beta bursts; and 2) the HG bursts. Analyses were performed within subjects. CNNs were implemented in Keras™ for binary classification of: 1) encoding vs recall iEEG epochs (CNNs #1, Figure 1); 2) good encoding vs. poor encoding iEEG epochs (CNNs #2, Figure 1C); and 3) good vs poor recall iEEG epochs (CNNs #3, Figure 1C). This input to the CNN included either the HG and beta time-series as two variables per contact (CNN#1,2,3), or the raw normalized iEEG alone (CNN#2) as a single variable per contact. The CNN #3 threshold, for a patient's good and poor recall classification, was derived as the mode of the distribution of total words recalled in each session, across sessions.

The CNN architecture used for all models consisted of pairs of Conv1D and Batch Normalization layers followed by a Global Average Pooling layer and the output layer. The CNN structure utilized was 3 convolutional one-dimensional layers, a Kernel size of three, and an Adam optimizer. Hyperparameter tuning was performed by utilizing several combinations of the number of convolutional layers and units per layer and maximizing the mean area under the receiver operating curve (AUC) across all subjects. The hyperparameters were: 1) 100 epochs and a batch size of 128 for CNN #1; 150 epochs and a batch size

size of 128 for CNN #1; 150 epochs and a batch size of 128 for analysis for CNN #2; and 100 epochs and a batch size of 32 for CNN #3. For each patient, the confusion matrices and related measures were derived using five-fold cross-validation across all the trials for CNN#1,2. In the case of CNN#3 two-fold cross-validation was used because of few trials. For individual subjects the free-recall and categorical free-recall experiments were analyzed separately.

Results

The data analyzed herein was generated during the Restoring Active Memory (RAM) project (Camarillo-Rodriguez et al., 2022; Ezzyat et al., 2018, 2017; Horak et al., 2017; Kucewicz et al., 2018, 2017). This project included hundreds of patients with medically refractory epilepsy undergoing pre-surgical evaluation. Each of the subjects performed the verbal free recall task (Figure 1A). The multisite collaborative DARPA RAM research team examined whether the iEEG, from all the recording contacts and all spectra of brain activity, can be used to train a logistic regression classifier to distinguish recalled words from forgotten words using the iEEG recorded during the encoding epoch. Using this methodology the mean area under the receiver operating curve (AUROC) was 0.63 +/- 0.07(Ezzyat et al., 2018, 2017). The logistic regression classifier utilized by the RAM study is analogous to CNN#2 implemented in our study that identified recalled words during the encoding epoch (Figure 1A,1B2). Our method was distinct, however, because training and testing of CNNs 1-3 relied solely on iEEG recordings from the left supramarginal gyrus (LSMG), and in certain experiments only bursts of high-gamma and beta recorded by contact in the LSMG (CNN#2b). The recordings from LSMG were either from depth electrode contacts, subdural strip or subdural grid contacts. As few as 2 and as many as 27 contacts were situated in or on the LSMG across the experiments.

In 142 experiments, we compared the AUROC of CNN#2a and CNN#2b (1A,1B2) that were trained and tested using the unfiltered LSMG iEEG (CNN#2a), or bursts of high-gamma (HG) and beta (CNN#2b), respectively, to classify remembered words during encoding. We found a strong linear correlation ($R2=0.22$, $p<0.001$) between the AUROC of CNN#2a and CNN#2b (Figure 2A). Comparing the AUROC of CNN#2a and CNN#2b in the subset of experiments (n=63) with an AUROC of CNN#2b greater than chance (AUROC>0.52, Figure 2B) indicated that for a subset of experiments, with an AUROC>0.6 (Figure 2B green and blue squares), the AUROC of CNN#2b (HG and beta bursts) exceeded the AUROC of CNN#2a (Figure 2B).

To investigate why CNN#2b predicted recalled words during encoding with an AUROC >60% in only a small number of subjects (n=14 blue, green squares, Fig 2B) we compared the AUROC of CNN#2b in individual experiments with the peak amplitude of the HG and beta bursts (Figure 2C). All 16 of the experiments with a CNN#2b AUROC>60% had either a peak HG>50uV or a peak beta>0.5mV (Figure 2C, green circles). Most other experiments with a CNN#2b AUROC<60% had a peak HG<50uV (Figure 2C, black circles). However, in six experiments (Figure 2C, red circles) the peak HG exceeded 50uV but the CNN#2b AUROC was <60%.

We hypothesized that the location of depth electrode contacts in the LSMG may differ for experiments with a CNN#2b AUROC>0.6 (Figure 2C, green circles) and experiments with a CNN#2b AUROC<0.6 but peak HG>100uV (Figure 2C, red circles). We found that the patients with a CNN#2b AUROC>0.6 had depth electrode contacts placed in the anterior-dorsal-most portion of the LSMG (Figure 2D2), whereas patients with a CNN#2b AUROC<0.6 but exhibiting HG>100uV had depth electrode contacts most posteriorly in the LSMG (Figure 2E). Additionally, we found that experiments in patients with subdural electrode implants and a CNN#2 AUROC>0.6 had coverage of most of the LSMG (Figure 2D1), except for the most posterior and inferior regions (Figure 2E). While high gamma and beta burst amplitude corresponded with a larger AUROC for CNN#2, we did not observe a linear correlation between the number of depth electrode contacts, subdural strip, subdural grids with a larger AUROC for CNN #2 ($p<0.05$).

Seven of our experiments with CNN#2 AUROC>0.6, peak HG>50 uV, and peak beta>0.5 mV, in seven subjects, had iEEG recordings during the recall epoch available (Figure 2B, blue squares). We next asked whether CNN#1 (Figure 1A,1B1), trained and tested using HG and beta bursts from a randomized combination of 3 second encoding epoch and recall trials, could accurately identify the encoding epochs from the randomized free recall epochs. We found that all seven subjects exhibited an AUROC>0.6 and two of the subjects an AUROC>0.9 (Table 1). The CNN#1 AUROC was superior to the subject's corresponding CNN#2b AUROC (Table 2), since only two subjects exhibited a CNN#2b AUROC>0.7 (Table 2). Lastly, we examined CNN#3 (Figure 1A,1B3), in the seven subjects, that utilizes HG and beta bursts in the iEEG during the recall epoch to classify whether the number of recalled words exceeds the mean. We found that only two of the

seven subjects exhibited a CNN#3 AUROC>0.6 (Table 3).

Discussion

Past attempts to derive biomarkers of memory performance during encoding of words for the verbal free recall task have examined iEEG across all frequency spectra and among electrode contacts in diverse brain regions simultaneously (Ezzyat et al., 2018, 2017). We found that in 126 of the 142 experiments CNN#2b, which utilizes high-gamma and beta bursts in the LSMG iEEG during encoding, exhibited an AUROC<0.6 for classifying remembered words. However, in 16 experiments, verbal memory states and performance were predicted by CNN#2b, as well as CNN#1 and CNN#3, with equivalent accuracy to the past approaches (Ezzyat, et al., 2018, 2017). These sixteen experiments were unique from the others because: 1) the electrode contacts were in the anterior and dorsal portions of the LSMG; and 2) higher amplitude HG and beta bursts were detected in those contacts.

Prior work has shown the presence of subsequent memory effects (SME) in the LSMG using both fMRI(Cabeza et al., 2008; Ciaramelli et al., 2008) and iEEG (Gonzalez et al., 2015; Rubinstein et al., 2021). Delineating a SME relies on averaging responses to a stimulus and consequently, many SMEs coincide with stimulus presentation. HG and beta burst analyses have been utilized to better understand working memory and add additional information such as the onset, offset, frequency and duration of the burst (Kucewicz et al., 2017; Lundqvist et al., 2016; Lundqvist and Wutz, 2022; Miller et al., 2018). In our approach, we did not utilize the frequency content of the discrete bursts in the HG or beta band. Nonetheless, we found that in experiments with a sufficient signal-to-noise ratio for HG and/or beta the burst analysis approach discriminated verbal memory states and performance with an AUROC~>0.6.

Our study had several shortcomings. We did not perform an importance analysis using the CNNs to identify the neuroanatomical subregions of the LSMG for distinct aspects of memory state and performance classification (Fawaz et al., 2019). Additionally, we did not derive activity maps that could identify the distinct temporal windows most important for classification (Fawaz et al., 2019). These additional analyses could be utilized in the future to better understand the algorithm utilized by the CNNs, and improve the CNNs used in this study. Lastly, while we compared the AUROC of CNN#2a, that utilized raw iEEG, with CNN#2b, utilizing HG and Beta bursts, we did not test a CNN that used all brain signals in tandem.

Understanding the neurophysiological correlates of verbal memory is better studied in epilepsy patients with intracranial electrodes as compared to scalp EEG (Long et al., 2014). Future research could examine whether sub-scalp electrode contacts (Duun-Henriksen et al., 2020) over the LSMG can detect HG and beta bursts with a sufficient signal-to-noise ratio to train and test the CNNs described herein.

Figures

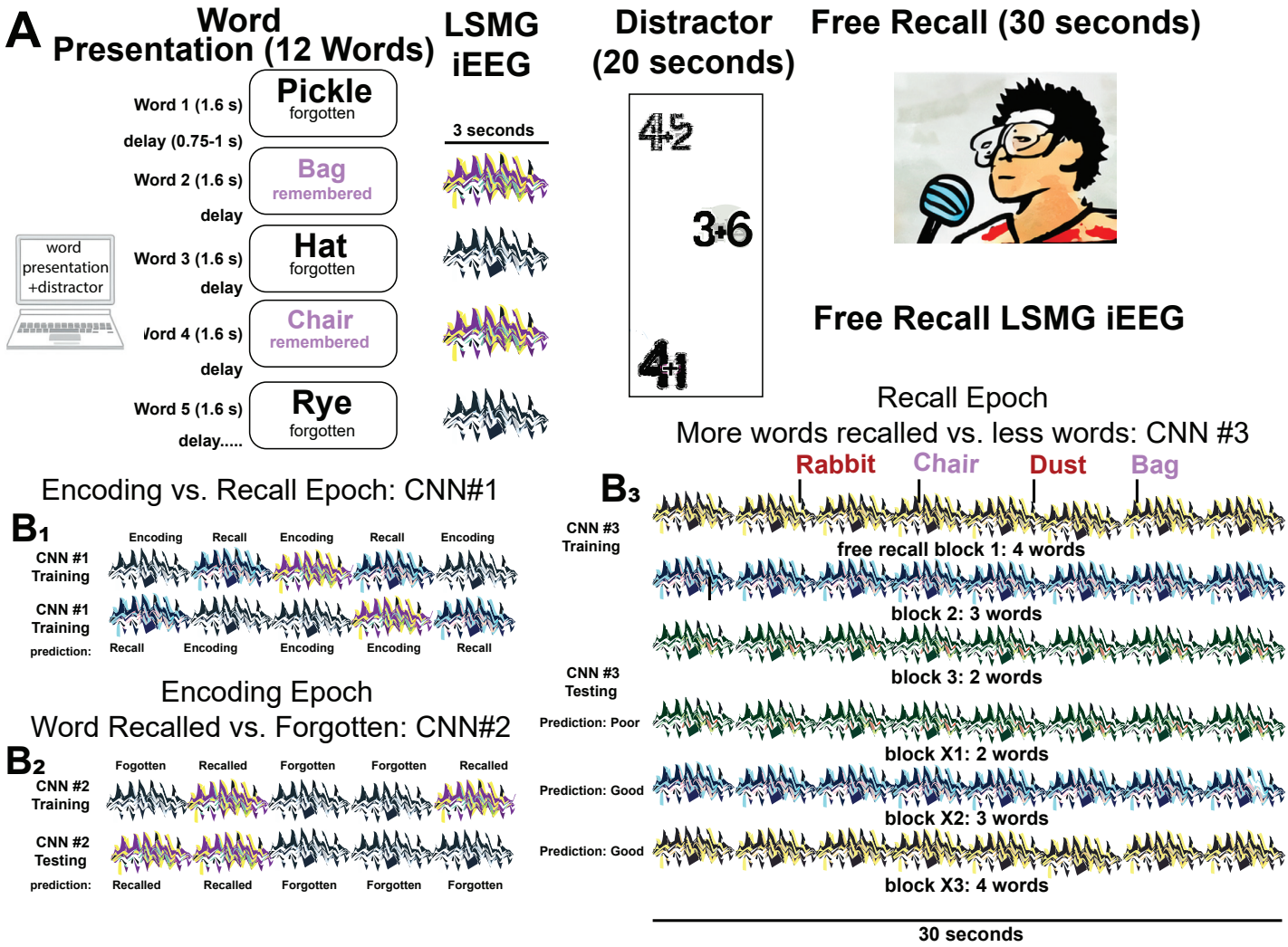

Figure 1: **Experimental design and illustration of convolutional neural networks (CNNs) training and testing.** A) The subjects participated in a verbal free recall task (encoding, distractor, and recall). First, the patient is instructed to remember a list of 12 words that are sequentially presented on a computer screen separated by an inter-word interval. After the 12 words are presented, participants solve simple arithmetic operations as a distractor. Lastly, the participant has 30 s to recall as many words as possible. In the experimental block shown the subject successfully encodes two words “Bag” and “Chair” (magenta). (B) Illustrations of the training and testing of the 3 CNNs using the color-coded multi-channel intracranial EEG (iEEG) recorded from the left supramarginal gyrus (LSMG) associated with the different tasks and the task performance (Key: black and white iEEG: encoding - forgotten; purple and yellow: encoding - recalled; black and green: recall - poor; black and blue: recall – good; black and green: recall – good). CNNs are trained using each trial’s and session’s corresponding iEEG, and the subject’s corresponding memory state and performance. Testing of the CNNs predicts the memory state and performance for each trial and block using the corresponding iEEG.

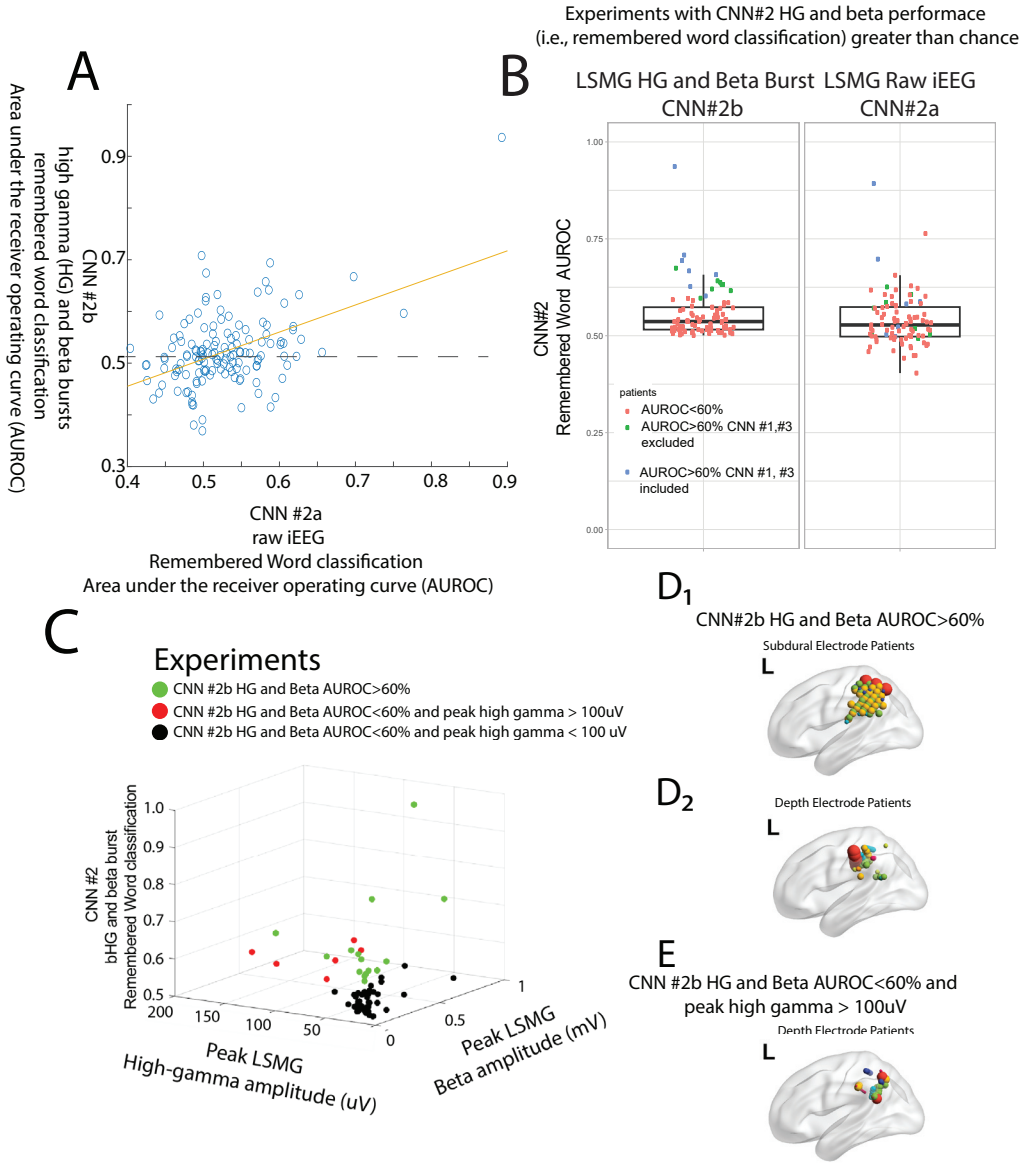

Figure 2: **During word encoding, higher amplitude high-gamma (HG) and beta bursts in the anterior region of the left supramarginal gyrus (LSMG) corresponds with improved performance of the trained convolutional neural network (CNN) in classifying recalled words.** (A) Within experiment comparisons of the area under the receiver operating curve (AUROC) for classifying remembered words utilizing raw iEEG to train and test the CNN on the x-axis and utilizing high-gamma (HG) and beta bursts to train and test the CNN on the y-axis (R2=0.22, p<0.001). (B) Among the experiments in which the CNN utilizing HG and beta burst classified remembered words better than chance (see A, dashed line), a boxplot of the CNN#2 AUROC when utilizing HG and beta (left) and corresponding raw iEEG (right) shows that in some experiments the HG and beta bursts were superior in performance. Experiments with a CNN#2 AUROC greater than 60% and sufficient data for training and testing CNN #1 (encoding vs. recall) and CNN #3 (good recall vs. poor recall) are shown as blue squares, whereas experiments with an AUROC greater than 60% and missing data are shown as green squares. (C) A comparison of the peak HG and beta power for each experiment and corresponding AUROC of CNN#2 utilizing HG and beta bursts. Green circles indicate experiments with an AUROC>60%, red circles patients with an AUROC<60% but peak high-gamma >100 uV, and black circles an AUROC<60% and peak high-gamma <100uV. (D) Location of electrode contacts (D1:subdural,D2:depth) for experiments with a CNN#2 HG and beta AUROC>60%. Colors indicate individual subjects, and larger size contacts represent larger AUROC values. (E) Location of depth electrodes for the subjects in (C, red circles) with larger HG amplitudes but AUROC<60%. Note that in the experiments in which CNN#2, utilizing HG and Beta, exhibited a >60% AUROC in classifying remembered words, the anterior-dorsal region of the LSMG was sampled in patients with depth and subdural recordings, respectively.

Tables

Table 1: Confusion table metrics of encoding vs. recall trial classification using high-gamma and burst inputs in the left supramarginal gyrus, during the encoding and recall epochs, for training and testing convolutional neural network #1 (CNN#1). Metrics calculated at Youden's J of the receiver operating curve.

Subject	accuracy	Auc	ppv	npv	sensitivity	specificity	f1	sessions
1	0.992	1.000	1.000	0.985	0.985	1.000	0.992	10
2	0.698	0.743	0.712	0.712	0.692	0.705	0.691	32
3	0.754	0.849	0.744	0.756	0.683	0.825	0.698	40
4	0.660	0.698	0.670	0.637	0.438	0.882	0.502	50
5	0.628	0.625	0.649	0.659	0.640	0.614	0.611	24
6	0.698	0.733	0.798	0.699	0.611	0.796	0.639	8
7	0.933	0.965	0.937	0.932	0.930	0.937	0.933	12

Table 2: Confusion table metrics of word remembered vs. word forgotten classification using high-gamma and burst inputs in the left supramarginal gyrus, during the encoding epoch, for training and testing convolutional neural network #2b (CNN#2b). Metrics calculated at Youden's J of the receiver operating curve.

Subject	Accuracy	Auc	ppv	npv	sensitivity	specificity	f1	sessions
1	0.629	0.606	0.177	0.915	0.605	0.576	0.252	40
2	0.637	0.613	0.200	0.897	0.534	0.654	0.282	24
3	0.701	0.715	0.376	0.877	0.560	0.732	0.413	10
4	0.637	0.613	0.200	0.897	0.534	0.654	0.282	24
5	0.620	0.642	0.142	0.947	,0.667	0.582	0.229	32
6	0.694	0.626	0.236	0.819	0.333	0.788	0.254	8
7	0.862	0.906	0.858	0.873	0.817	0.894	0.834	50

Table 3: Confusion table metrics of more words remembered vs. less words remembered classification using high-gamma and burst inputs in the left supramarginal gyrus, during the recall epoch, for training and testing convolutional neural network #3 (CNN#3.) Metrics calculated at Youden's J of the receiver operating curve.

Subject	accuracy	Auc	ppv	npv	sensitivity	specificity	f1	sessions
1	0.567	0.575	0.208	0.658	0.300	0.700	0.243	40
2	0.840	0.860	0.947	0.693	0.828	0.871	0.876	24
3	0.613	0.440	0.162	0.730	0.260	0.746	0.196	10
4	0.557	0.479	0.351	0.643	0.400	0.658	0.329	24
5	0.520	0.508	0.350	0.517	0.317	0.733	0.313	32
6	0.583	0.543	0.494	0.606	0.530	0.626	0.487	8
7	0.724	0.790	0.728	0.775	0.709	0.736	0.683	50

Credit author statement: **Nicolás Sawczuk** - conceptualization, methodology, software, investigation, resources, writing – original draft, writing – review & editing. **Daniel Y. Rubinstein** software, investigation, resources, writing – original draft, writing – review & editing. **Michael R. Sperling -** investigation, writing – review & editing, funding acquisition. **Katrina Wendel-Mitoraj -** review & editing. **Diego F. Slezak -** investigation, writing – review & editing, funding acquisition. **Juan Kamienkowski -** investigation, writing – review & editing, funding acquisition. **Shennan Aibel Weiss** - conceptualization, methodology, software, investigation, resources, writing – original draft, writing – review & editing

Funding
This work was supported by Defense Advanced Research Projects Agency (DARPA) grant N66001-14-2-4032. DARPA was not involved in study design, data collection, data analysis, data interpretation, report writing, or decision to submit for publication. The views, opinions, and/or findings contained in this material are those of the authors and should not be interpreted as representing the official views or policies of the US Department of Defense or the US Government. No funding source supported the secondary analysis of this data.

Acknowledgements
The authors would like to thank Dr. Camarillo-Rodriguez, Mr. Zachary Waldman, Dr. Paul Wanda, Dr. Michael Kahana, Dr. Daniel Rizzuto, Dr. Sandhitsu Das, Dr. Iren Orosz, Dr. Ashwini Sharan, Dr. Joel Stein, Dr. Bradley Lega, Dr. Robert Gross, Dr. Gregory Worrell, Dr. Katherine Davis, Dr. Barbara Jobst, Dr. Sameer Sheth.

Conflict of Interest
S.A.W, N.S, J.K, and D.S are inventors on a related provisional patent 63/621,314. S.A.W and M.S. are inventors of granted patent US20240090817A1. M.R.S. is a consultant/advisor for Medtronic (fee to institution); has received research support (to institution) from Eisai, Engage Therapeutics, Medtronic, Neurelis, Pfizer, SK Life Science, Takeda, UCB, Cerevel, and Xenon; and has been a speaker for Eisai, Medscape, NeurologyLive, UCB, and Projects in Knowledge. K.W.M is the CEO and founder of Soenia®.

Data availability
Please see the methods section for hyperlinks to the opensource dataset. The code used in this analysis is freely available upon reasonable request to the authors.

References

Bernard F, Lemee J, Mazerand E, Leiber L, Menei P, Minassian AT (2020) The ventral attention network: the mirror of the language network in the right brain hemisphere. J Anat 237:632–642.

Cabeza R, Ciaramelli E, Olson IR, Moscovitch M (2008) The parietal cortex and episodic memory: an attentional account. Nat Rev Neurosci 9:613–625.

Camarillo-Rodriguez L, Leenen I, Waldman Z, Serruya M, Wanda PA, Herweg NA, Kahana MJ, Rubinstein D, Orosz I, Lega B, Podkorytova I, Gross RE, Worrell G, Davis KA, Jobst BC, Sheth SA, Weiss SA, Sperling MR (2022) Temporal lobe interictal spikes disrupt encoding and retrieval of verbal memory: A subregion analysis. Epilepsia 63:2325–2337.

Canolty RT, Edwards E, Dalal SS, Soltani M, Nagarajan SS, Kirsch HE, Berger MS, Barbaro NM, Knight RT (2006) High Gamma Power Is Phase-Locked to Theta Oscillations in Human Neocortex. Science 313:1626–1628.

Ciaramelli E, Grady C, Levine B, Ween J, Moscovitch M (2010) Top-Down and Bottom-Up Attention to Memory Are Dissociated in Posterior Parietal Cortex: Neuroimaging and Neuropsychological Evidence. J Neurosci 30:4943–4956.

Ciaramelli E, Grady CL, Moscovitch M (2008) Top-down and bottom-up attention to memory: A hypothesis (AtoM) on the role of the posterior parietal cortex in memory retrieval. Neuropsychologia 46:1828–1851.

Duun-Henriksen J, Baud M, Richardson MP, Cook M, Kouvas G, Heasman JM, Friedman D, Peltola J, Zibrandtsen IC, Kjaer TW (2020) A new era in electroencephalographic monitoring? Subscalp devices for ultra–long-term recordings. Epilepsia 61:1805–1817.

Ezzyat Y et al. (2018) Closed-loop stimulation of temporal cortex rescues functional networks and improves memory. Nat Commun 9:365.

Ezzyat Y et al. (2017) Direct Brain Stimulation Modulates Encoding States and Memory Performance in Humans. Curr Biol 27:1251–1258.

Fawaz HI, Forestier G, Weber J, Idoumghar L, Muller P-A (2019) Deep learning for time series classification: a review. Data Min Knowl Discov 33:917–963.

Gonzalez A, Hutchinson JB, Uncapher MR, Chen J, LaRocque KF, Foster BL, Rangarajan V, Parvizi J, Wagner AD (2015) Electrocorticography reveals the temporal dynamics of posterior parietal cortical activity during recognition memory decisions. Proc National Acad Sci 112:11066–11071.

Horak PC et al. (2017) Interictal epileptiform discharges impair word recall in multiple brain areas. Epilepsia 8:373–380.

Kucewicz MT et al. (2018) Evidence for verbal memory enhancement with electrical brain stimulation in the lateral temporal cortex. Brain 141:971–978.

Kucewicz MT, Berry BM, Kremen V, Brinkmann BH, Sperling MR, Jobst BC, Gross RE, Lega B, Sheth SA, Stein JM, Das SR, Gorniak R, Stead SM, Rizzuto DS, Kahana MJ, Worrell GA (2017) Dissecting gamma frequency activity during human memory processing. Brain 140:1337–1350.

Long NM, Burke JF, Kahana MJ (2014) Subsequent memory effect in intracranial and scalp EEG. NeuroImage 84:488–494.

Lundqvist M, Rose J, Herman P, Brincat SL, Buschman TJ, Miller EK (2016) Gamma and Beta Bursts Underlie Working Memory. Neuron 90:152–164.

Lundqvist M, Wutz A (2022) New methods for oscillation analyses push new theories of discrete cognition. Psychophysiology 59:e13827.

ller EK, Lundqvist M, Bastos AM (2018) Working Memory 2.0. Neuron 100:463–475.

Mukamel R, Gelbard H, Arieli A, Hasson U, Fried I, Malach R (2005) Coupling Between Neuronal Firing, Field Potentials, and fMRI in Human Auditory Cortex. Science 309:951–954.

Rubinstein DY, Camarillo-Rodriguez L, Serruya MD, Herweg NA, Waldman ZJ, Wanda PA, Sharan AD, Weiss SA, Sperling MR (2021) Contribution of left supramarginal and angular gyri to episodic memory encoding: An intracranial EEG study. Neuroimage 225:117514.

Sestieri C, Shulman GL, Corbetta M (2017) The contribution of the human posterior parietal cortex to episodic memory. Nat Rev Neurosci 18:183–192.

Sinai A, Bowers CW, Crainiceanu CM, Boatman D, Gordon B, Lesser RP, Lenz FA, Crone NE (2005) Electrocorticographic high gamma activity versus electrical cortical stimulation mapping of naming. Brain 128:1556–1570.

Uncapher MR, Wagner AD (2009) Posterior parietal cortex and episodic encoding: Insights from fMRI subsequent memory effects and dual-attention theory. Neurobiol Learn Mem 91:139–154.

Waldman ZJ, Shimamoto S, Song I, Orosz I, Bragin A, Fried I, Engel J, Staba R, Sperling MR, Weiss SA (2018) A method for the topographical identification and quantification of high frequency oscillations in intracranial electroencephalography recordings. Clin Neurophysiol 129:308–318.

Yagmurlu K, Middlebrooks EH, Tanriover N, Rhoton AL (2016) Fiber tracts of the dorsal language stream in the human brain. J Neurosurg 124:1396–1405.